RSC Advances

ROYAL SOCIETY OF CHEMISTRY

www.rsc.org/advances

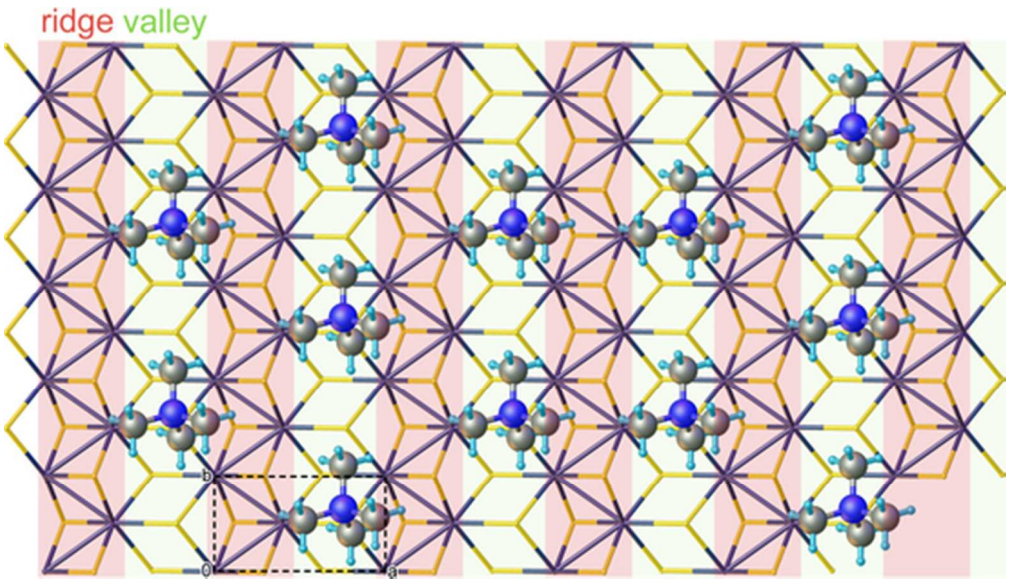

Graphical abstract
46x26mm (300 x 300 DPI)

Ridges and Valleys on Charged 1T-MoS_2 Sheets Guiding the Packing of Organic Cations

Alexander S. Goloveshkin[†], Natalia D. Lenenko[†], Vladimir I. Zaikovskii[‡,§], Alexandre S. Golub[†], Alexander A. Korlyukov[†], Ivan S. Bushmarinov[†]*

[†]A.N. Nesmeyanov Institute of Organoelement Compounds, Russian Academy of Sciences, 119991, 28 Vavilova St., Moscow, Russia; [‡]Boreskov Institute of Catalysis, Siberian Branch of RAS, 630090, 5 Lavrentieva Ave., Novosibirsk, Russia; [§]Novosibirsk State University, 630090, 1 Pirogova St., Novosibirsk, Russia

TOC Entry

The three-dimensional atomic structure of MoS_2-organic layered systems is obtained for the first time, providing insight into the surface chemistry of charged MoS_2 sheets.

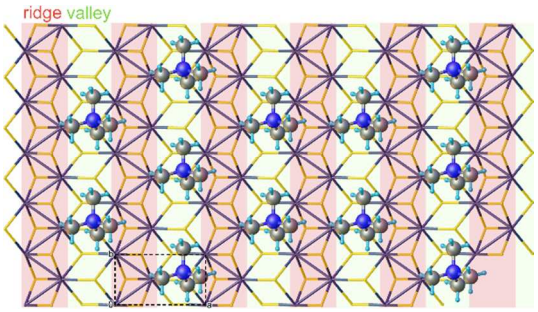

Abstract

Using a novel powder X-ray pattern refinement technique, DFT calculations and TEM, we reveal for the first time the three-dimensional structure of hybrid $(R_4N)_xMoS_2$ layered compounds. Both the precise coordinates of Mo and S atoms in the inorganic layer and the preferred positions of the organic cations relative to them are reported. The distorted geometry of the MoS_2 sheet is found to be the driving force behind the arrangement of cations within the organic layers. The refined atomic coordinates, confirmed by periodic DFT modeling, show octahedral Mo atoms arranged in zigzag chains and the S atoms following the Mo ones, forming “ridges” and “valleys” on the sheet surface. The size of alkylammonium cations is

compatible with these valleys, leading to a strong preferred arrangement: the cations exclusively occupy the space between the ridges. This result allows predicting the layer structure and ultimately the composition of the hybrid compound depending on the cation structure. The reported features of the MoS_2 surface are important for understanding of MoS_2-based sensors and hybrid flexible conductors, both relying on charged sheets of MoS_2.

1. Introduction

Molybdenum disulfide is an important graphene analog demonstrating semiconducting properties both in bulk[1] and as single layers.[2]

A single layer of molybdenum disulfide consists of fused MoS_6 polyhedra forming a flat, three atoms thick S-Mo-S sandwich[3]. Like graphene, these 2D sheets, both monolayerly thin[2,4] or assembled in few-layer particles,[5,6] are considered particularly important components for future nanoelectronic devices,[2,4,6] sensors,[7,8] and electrocatalysts.[9] Chemical modification of 2D materials like graphene or molybdenum disulfide due to their non-covalent interactions with donor or acceptor molecules is a promising route to fine-tuning their properties for different applications.[6,7,10–12]

The unique feature of the MoS_2 layers is the susceptibility of their atomic structure and properties to negative charge transferred onto layers. This charge induces atomic rearrangements[13–17] and changes behavior of the resulting material from semiconducting to metallic.[17–19] The process is usually referred as “2H to 1T phase transition”, but the actual rearrangement may involve at least three separate transitions between structurally distinct phases.[20] Several MoS_2 forms were also directly observed in metal-doped MoS_2 under the beam of electronic microscope.[21] The fully lithiated MoS_2 displays a octahedral modification with Mo atoms organized in ‘diamond’ formation,[15] while Na_xMoS_2 exhibits 2H, 1T and several 1T-based modulated phases depending on the value of x.[22]

Still, the detailed structural studies in the literature are limited to purely inorganic systems. As for MoS_2-organic intercalation compounds, the form of MoS_2 and the arrangement

of the cations relative to the inorganic layers remain unknown and their elucidation is the main goal of this manuscript.

Hybrid MoS_2-based heterostructures where organic cationic species[16,23–26] (B^+) are sandwiched between negatively charged sulfide layers are prepared by using the negatively charged MoS_2 sheets as building blocks in self-assembly process (eq. 1). The resulting particles are 2-10 layers thick.[24,25]

$$MoS_2 \xrightarrow[B^+]{Li^+,\ e^-} Li^+(MoS_2)^- \xrightarrow{H_2O} [Li^+ + (MoS_2)^{x-} + (1-x)OH^-]_{aq} \longrightarrow (B^+)_x(MoS_2)^{x-} \quad (1)$$

The hybrid $(B^+)_x(MoS_2)^{x-}$ compounds with alkylammonium cations easily form flexible conductive films.[23,24] As intermediates, they find use in preparation of various mesoporous MoS_2-based materials.[27,28]

Studies of similar substances by XRD, EXAFS[14,16], PDF[15], TEM,[17,29] electron diffraction[18,29] together with quantum-chemical calculations[30,20] revealed that rearrangements of S-Mo-S network induced by the charge transfer lead to formation of molybdenum zigzag chains and probably change the MoS_6 polyhedra from trigonal prisms (neutral layers) to octahedra (negatively charged layers). However, to the best of our knowledge, structures of hybrid MoS_2-organic layered compounds have been neither resolved at the atomic level by any method nor successfully modeled using quantum-chemical approaches.

The obvious method for determination of the 3D structure of a substance is X-ray diffraction. Unfortunately, the MoS_2-based hybrid compounds do not form single crystals, and their powder XRD patterns contain very few sharp peaks required for typical Rietveld refinement. The usually reported and easily measurable *00l* reflections provide only the periodicity in the direction normal to the sulfide sheets and reveal neither the actual positions of the guest molecules between MoS_2 layers nor the exact MoS_2 layer structure. However, the

modern developments in the X-ray diffraction theory allow going beyond sharp peaks in the analysis of the powder patterns. The aim of the current study was to extract novel structural information from the full powder patterns of hybrid MoS_2 materials.

The tetramethyl- and tetraethylammonium layered salts $(Me_4N)_{0.25}MoS_2$ and $(Et_4N)_{0.15}MoS_2$, further referred to as **TM** and **TE** respectively, were chosen for detailed study due to their reproducible composition and symmetric guest moiety.

2. Results and discussion

2.1. Structural studies

The diffraction patterns of **TM** and **TE** are visually similar, consisting of strong symmetric *00l* lines and broad reflections of different origin (**Figure 1**). The strong 00l lines indicate that the studied compounds are indeed three-dimensional, and not monolayerly thin.[31] Besides the reflections in 2θ>30 region, both patterns contain a weak peak at ≈15.5° 2θ, which does not change position despite the difference in interlayer (00l) distance (11.1733(2) Å in **TE** and 11.0620(3) Å in **TM**). This peak, along with other non-00l peaks in the patterns, was indexed in *pg* plane group with a=5.6991(12) and b= 3.2001(10) Å (see SI for details). These values, corresponding approximately to $(\sqrt{3}a, a)$, where *a* is the unit cell parameter of crystalline[15] 2H-MoS_2, indicate the presence of the 2x1 supercell often found[32] in charged MoS_2 layers. More notable is the complete absence of the *hkl* peaks; along with the asymmetric shape of the "plane group" peaks, it indicated that the materials are turbostratically disordered in a manner similar to clays or carbon black.[33] In these structures, layers can move and rotate freely against each other, the *hkl* peaks disappear, and the *hk0* peaks become *hk* diffraction bands, while the diffraction along the 00l direction still shows normal Bragg reflections.

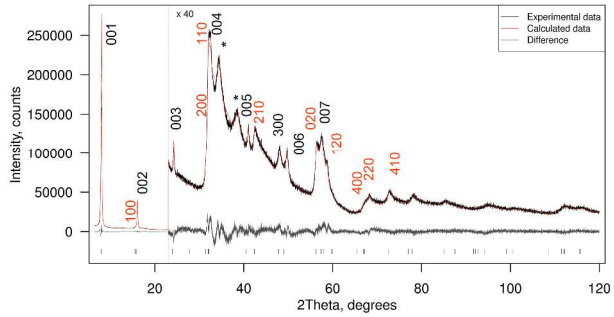

(a)

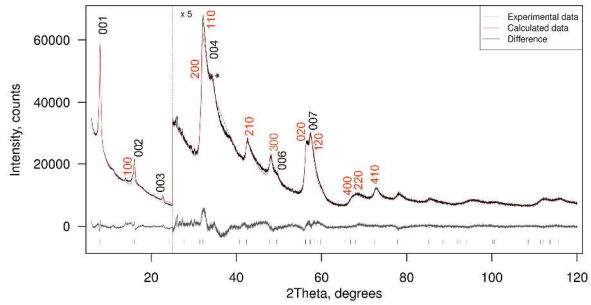

(b)

Figure 1. The fit of TE (a) and TM (b) powder patterns using the approach outlined in 4.2. Refinement model. Diffraction bands are labeled in red, stars denote the independently refined peaks, and ticks label the *00l* and *hk0* positions.

There have been reports[34–36] of quantifying the mixtures containing similarly disordered clays using a specially created supercell with scaled reflection intensities to represent the clay phase. In this work, we repurposed this approach for true structure refinement of the $(R_4N)_xMoS_2$ structure, both of the MoS_2 sheet and of the organic layer, simultaneously including the sharp *00l* peaks and wide *hk* bands in the fit (see 4.2. Refinement model). To our knowledge, the current work is the first application of this model to MS_2 structures or to any system except clays. The main advantage before the more commonly[37] used Debye formula modeling is the possibility of direct least squares refinement of the studied structure.

Initially, atomic positions from 2H-MoS_2 were used as starting coordinates for the refinement of the inorganic layer geometry. The models for both **TM** and **TE** converged to

similar distorted layer structures with zigzag ordering of the Mo atoms, but the unusually close S…S distances and unsatisfying fit led to rejection of this model (See Supporting Information for refinement details).

Thus, we assumed octahedral[14] coordination of Mo atoms (called 1T-MoS_2 in the case of the exotic[38] bulk crystalline species). The crystal structure of pure 1T-MoS_2 has never been published, so we started the refinement with sulfur atoms approximately shifted to octahedral positions. It led to a reasonable structural model with a significantly better fit (**TE** R_{wp} of 4.339 as compared to 5.762 in the distorted prismatic model).

The main features of the resulting structure, distinguishing it from the idealized octahedral one, are zigzag chains of the Mo atoms (**Figure 2**) and pronounced displacement of the sulfur atoms (**Figure 3**): the S atoms bound to only one Mo chain form 'ridges', and sulfur atoms linking two different chains form 'valleys' between. These S-S-S valleys are ≈ 0.5 Å deep, and their effective width matches one of a CH_2 group (see **Figure 3**). As an external check, the refined Mo-Mo distances for **TM** (**Table 1**) agreed well with the EXAFS data reported in the literature[16] (3.76 Å, 3.15 Å, 2.77 Å). Also this structure is in line with published quantum-chemical calculations[32] indicating that the removal of Li from fully-lithiated MoS_2 leads to metastable ZT-MoS_2 with similar arrangement of atoms, since **TM** is produced *via* $LiMoS_2$.

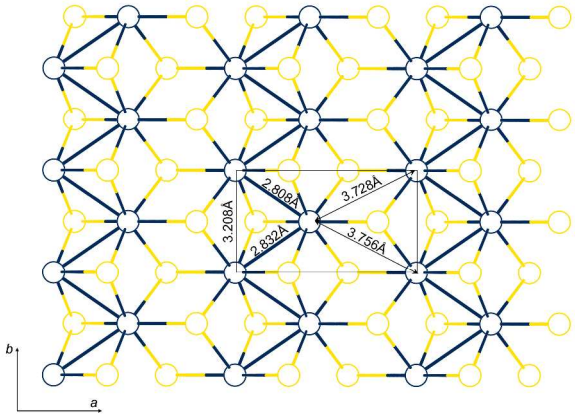

Figure 2. The MoS_2 layer structure of TE in the distorted octahedral model (final), view in the c direction. Rectangle denotes the refined supercell, Mo-Mo distances are labeled. Et_4N cation is omitted for clarity.

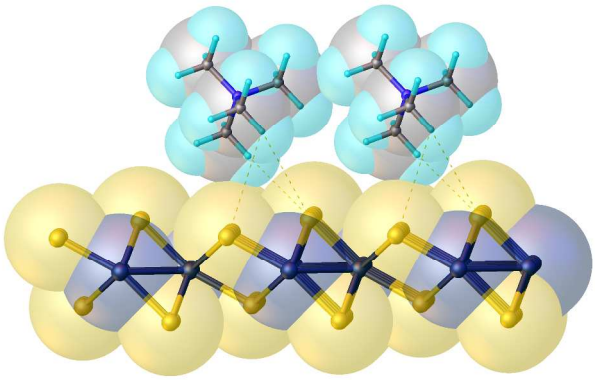

Figure 3. TM structure, view in the *b* direction. The spacefill model represents the van der Waals radii of the corresponding elements.

Along with the MoS_2 layer geometry, the refinement revealed the coordinates of the organic moiety within the unit cell: both in **TM** and **TE**, organic cations lie in the valleys between the Mo-Mo zigzags. The least squares procedure provided only approximate average occupancies of organic moiety due to correlations with Debye-Waller factor. To obtain precise occupancies and further insight into organic layer structure, we studied possible layer packings by placing maximum number of cations into refined positions on the MoS_2 sheet while avoiding collisions (**Figure 4**).

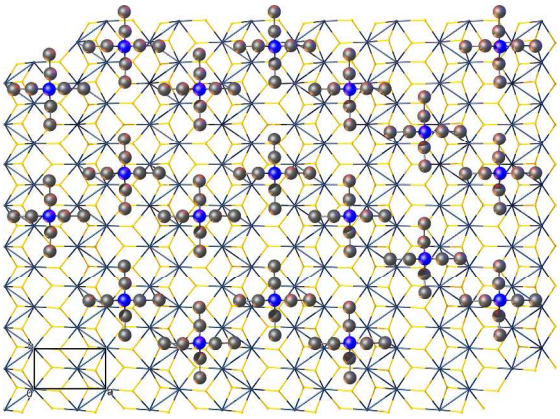

(a)

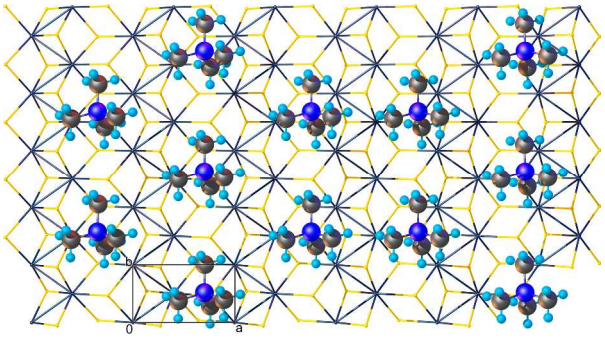

(b)

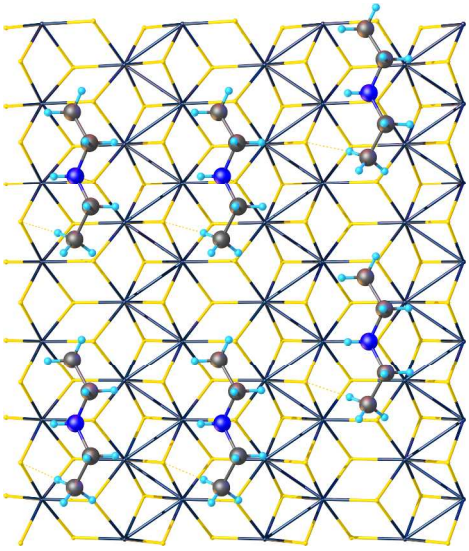

(c)

Figure 4. Example organic layer packing without long-range ordering, generated by expanding experimental unit cells (black rectangle) and randomly removing colliding cations, for TE (a), TM (b) and DE (c). Hydrogen atoms in TE are omitted for clarity.

Table 1. The summary of TM and TE final refinements in the distorted octahedral model.

	TE	TE calculated[a]	TM	DE
Composition	$(Et_4N)_{0.15}MoS_2$	$(Et_4N)_{1/6}MoS_2$	$(Me_4N)_{0.25}MoS_2$	$(Et_2NH_2)_{0.16}MoS_2$
a, Å	5.6924(5)	5.6924	5.6925(5)	5.7098(13)
b, Å	3.2083(3)	3.2083	3.2126(3)	3.2187(8)
c, Å	11.168(4)	11.168	11.096(5)	10.017(7)
R_{bragg}, %	1.380	-	1.714	1.944
R_{wp}, %	4.507	-	3.542	4.543
Mo-Mo distances, Å	2.808(7); 2.832(8) 3.2083(3) 3.737(6); 3.756(6)	2.835 3.220 3.753	2.789(6); 2.800(6) 3.2126(3) 3.762(4); 3.771(4)	2.852(6); 2.873(6) 3.2187(8) 3.715(5); 3.731(5)
Mo-Mo-Mo, °	69.35(4)	69.1	70.2(2)	68.42(5)
Mo-S, Å	2.400(5)	2.441	2.400(5)	2.400(5)
Valley depth[b], Å	0.527(5)	0.385	0.561(3)	0.548(5)

[a]Values provided are averaged over the 3x3x1 supercell used in the computation. [b]Calculated as $z_{S_{ridge}} - z_{S_{valley}}$

As we found out, the idealized composition of the organic layers can be estimated by counting the amount of cations fitting in the valleys without violation of the typical intermolecular distances. Optimal C…C contact distance between tetraalkylammonium cations is 3.2 Å according to CSD,[39] allowing one cation per two unit cells in **TM** and one per three in **TE** (**Figure 4**). Each unit cell contains two Mo atoms and four S, predicting R_4N/MoS_2 ratio of 0.17

for **TE** and 0.25 for **TM**, equal to the experimental composition within the precision of the chemical analysis. The tetraethylammonium cation is large enough to restrict cation placement not only in its "own" valley, but also in the neighboring ones; still, a favorable diagonal arrangement resulting in complete filling of all valleys is possible. It should be noted that above rules define only the local ordering and do not impose any additional long-range periodicity, as can be seen on **Figure 4**.

Analysis of **TM** and **TE** strongly suggests that the structure of the organic layer is determined by the ridges and valleys on MoS_2 surface and not simply by dense packing of the cations in a given space between "flat" MoS_2 sheets. This hypothesis was checked by preparing the salt of diethylammonium cation and MoS_2 (**DE**) and analyzing its composition and structure. Indeed, the $Et_2NH_2^+$ cation has the same atom count and volume as Me_4N^+, so we could expect a composition with 0.25 cations per MoS_2 formula unit in the case of dense packing of the organic layer. The diethylammonium cation, however, should occupy the same space as Et_4N^+ when fitted within a MoS_2 valley, leading to maximum 1/6 cations per MoS_2 if these valleys play the major role. The experimental composition, with 0.16 cations per MoS_2 unit, supports the latter model.

The fit of the **DE** experimental powder pattern using the same method as **TE** and **TM** (see Supporting Information) also confirms that the linear $Et_2NH_2^+$ fragments occupy the space in the valleys of distorted 1T-MoS_2.

2.2. DFT modeling and bonding analysis

In order to verify the refined geometry and quantify the cation-MoS_2 and cation-cation interactions, we aimed to model the hybrid MoS_2 system using *ab initio* calculations with periodic boundary conditions. The practically feasible computation methods are unsuitable for turbostratically disordered structures, so we constructed an ordered, 3D periodic model to approximate the experimental data using plane wave-based periodic DFT.

Due to the interactions between cations in neighboring valleys, the cation layer packing in **TE** is the most ordered among the studied compounds. This fact allowed assembling a

reasonable periodic approximation of the refined structure using only the [X+1, Y+1, Z] operation to fit the cation rows together and ignoring the turbostratic disorder (see Supporting Information for computational details). This very simplified model still reproduced the experimental Mo layer geometry, including the ridges and valleys, with high precision; the difference in refined and calculated bond lengths was similar to one usually achieved for calculations based on experimental single crystal data (**Table 1**).

The calculated structure was additionally studied using the R.F.W. Bader's quantum theory of atoms in molecules (QTAIM).[40] This theory reveals bonding interactions and charge transfer using topological analysis of the total electron density $\rho(\mathbf{r})$. In addition, the energy of weak interactions can be estimated using Esminosa-Molins-Lecomte (EML) correlations initially developed for weak hydrogen bonds[41–43] but further applied to a wide range of interactions,[44] including those in 2H-MoS_2.[45]

Table 2. Summary of average critical point properties (a.u.) in the 3x3x1 supercell of hypothetical ordered TE, according to PW-PBE-d modeling.

		Count	d, Å	$\rho(\mathbf{r})$	$\nabla^2\rho(\mathbf{r})$	$g_e(\mathbf{r})$	$v_e(\mathbf{r})$	$h_e(\mathbf{r})$	E_{EML}, kcal/mol
Mo	S	36	2.398	0.096	0.176	0.087	-0.130	-0.043	-40.6
Mo	S	36	2.433	0.090	0.157	0.078	-0.118	-0.039	-36.9
Mo	S	36	2.492	0.082	0.132	0.066	-0.100	-0.033	-31.2
Mo	Mo	18	2.835	0.057	0.087	0.039	-0.056	-0.017	-17.5
H	S	54	3.065	0.007	0.020	0.004	-0.003	0.001	-1.0
H	H	39	2.447	0.008	0.028	0.006	-0.004	0.001	-1.4

Each cation forms on average 18 S…H contacts with the MoS_2 layers, totaling 18.0 kcal/mol of interaction energy, and 13 H…H contacts with neighboring cations, for 18.2 kcal/mol total (**Table 2**). Thus the interactions within the organic layer are of similar importance for the formation of the structure as the interlayer ones, explaining the stable

stoichiometry of MoS_2 hybrid compounds. The organic cations also stabilize the MoS_2 layer by charge transfer (0.17 e per cation, measured by integration of $\rho(\mathbf{r})$ over the QTAIM atomic basins). Indeed, excess $LiMoS_2$ in the reaction mass leads to a two-phase system containing hybrid layered compound and 2H-MoS_2 instead of a single hybrid phase with lowered organic content.

2.3. Transmission electron microscopy studies

The **TE** compound, as the most stable one of the studied, was additionally examined using TEM. In agreement with the powder diffraction data, most particles of the material are turbostratically disordered, leading to HRTEM images in the basal projection similar to **Figure 5**. This came as a major limitation in our study, meaning that we could analyze only periodic or single-layer fragments in detail, without guarantee that their structure was similar to the bulk of the material: average thickness of the diffracting particles estimated by powder diffraction exceeds 200 nm (20 MoS_2 layers).

This problem of representativeness of basal projections of these particles became obvious during the examination of the visibly ordered images. The particles fell into two groups: purely hexagonal ones with period of 2.7 Å (See Supporting Information, Figure S2) and those with grouping of the spots in twin rows, corresponding to a superperiod of ≈5.75 Å (**Figure 7**d). The former can be attributed to 2H-MoS_2 while the latter can only be modeled using the layer structure obtained from XRD data (**Figure 7**b,c).

The powder patterns of **TE** show no presence of 2H-MoS_2. However, according to previous studies, heating of exfoliated-restacked MoS_2 to 400 K in vacuum leads to 2H-MoS_2 phase,[46,17] and processes of degradation for intercalated MoS_2 particles were observed in the MoS_2 — long-chain alkylammonium system under electronic beam.[25]

The FFT processing of the TEM side projections of the studied particles provides d_{001} distances ranging from 9.16 Å to 11.66 Å (**Figure 6**). The mean c-value obtained by refinement of XRD patterns (11.168 Å) lies near the upper end of this range.

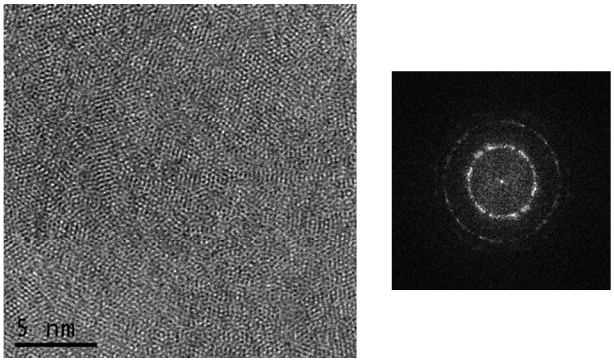

Figure 5. The TEM image of a turbostratically disordered TE particle (basal projection) and its FFT (on the right).

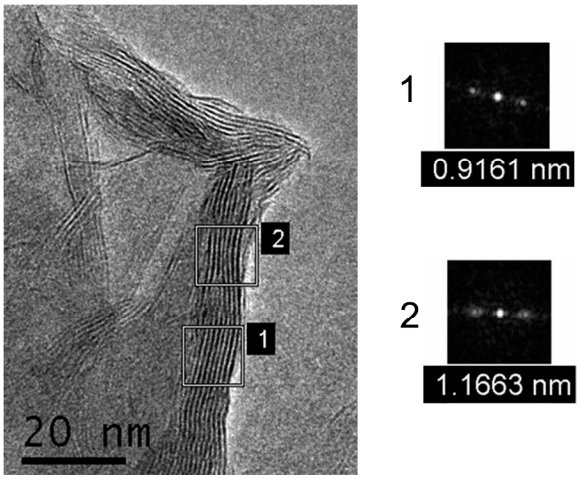

Figure 6. The TEM image of the side projection of TE and FFT transforms of its fragments with corresponding period values.

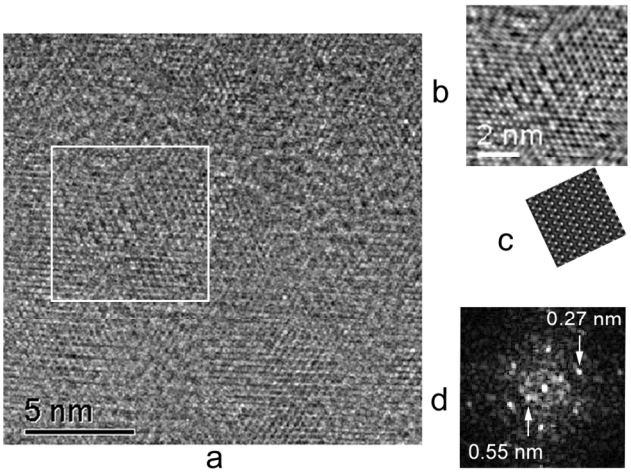

Figure 7. The HRTEM image for a particle with a superperiod (a), its magnified fragment (b) and contrast function simulated from the TE distorted octahedral structural model (c) (modeling parameters: lens defocussing of 63.0 nm, crystal thickness of 28.6 nm); FFT from selected area on "a" (the reflections d_{200} = 0.27 nm and d_{100} = 0.55 nm for TE are labeled)

The TEM results confirm the presence of hybrid layered compound and of MoS_2 layers showing distorted octahedral structure among the particles of **TE**. Still, we cannot exclude the possibility that this structure coexists with the prismatic modification similar to 2H-MoS_2, at least in the few-layer samples subjected to electronic irradiation in the microscope. Recently, coexistence of the domains with 1T (octahedral) and 2H (trigonal prismatic) modifications was revealed in TEM studies of MoS_2 layers obtained by removal of Li from $LiMoS_2$[17] or partial lithiation.[32]

3. Experimental

3.1. Materials synthesis

Layered compounds of MoS_2 with tetramethyl-, tetraethyl- and diethylamonium cations were obtained according to procedure described elsewhere.[47] Experimental details of synthese, TEM and powder X-ray diffraction measurements are presented in the Supporting information.

3.2. Refinement model

For structure refinement of PXRD patterns of **TM**, **TE** and **DE** we applied the X. Wang implementation[35,36] for TOPAS 4.2[48] of the "supercell approach" developed by K. Ufer *et. al.*[34] This model relies on the similarity between diffraction from single layers and turbostratically disordered structures. It describes the *hk* rods and the outline of the corresponding *hk0* diffraction bands in the powder pattern by a periodic unit cell of a special form: a "virtual" supercell elongated by a factor N≥10 in the stacking direction, containing one unit cell of the hypothetical ordered structure and N-1 empty unit cells. After removing the *00l* reflections with $l \not\equiv 0 \pmod N$ and scaling the intensity of the remaining *00l* reflections by N, the model provides a simultaneous description of the *hk0* bands and *00l* peaks.

It is important to state explicitly that shifts and rotations of the layers against each other are not refined and are not even present in the model, assuming a complete absence of positional correlation. The refinement details regarding the line broadening functions,

preferred orientation correction and Mo-S restraints can be found in the Supporting information.

The hypothetical "ordered" crystal structures have been deposited with CCDC (refcodes 1035816-1035818).

Supporting Information. Experimental details of syntheses, TEM, powder X-ray diffraction measurements and calculations; CIF files, calculated geometry data, powder datasets.

4. Conclusion

Both the MoS_2 sheet structure and the positions of organic cations in MoS_2-organic hybrid materials were reconstructed from powder X-ray diffraction patterns of these turbostratically disordered compounds. The refinement results were verified by periodic DFT calculations and confirmed by TEM.

The studied compounds demonstrate distorted octahedral (1T) geometry of the MoS_2 sheets, with 2x1 orthorhombic supercell as a repeating unit and Mo atoms forming zigzag chains.

The important new feature compared to previously reported structures of similar materials are the displacements of the sulfur atoms: the S atoms above Mo zigzags form 'ridges' and between these ridges lie 'valleys' 0.5 Å deep. Most notably, the width of the 'valleys' is complementary for a CH_2 or a CH_3 group, leading to organic cations packing exclusively in the valleys. This preference is the main cause behind the composition of the studied materials: the amount of cations per MoS_2 unit in the organic layer is determined not by dense packing of the organic cations, but by the amount of the cations fitting in the valley. At the same time, the space above 'ridges' is strongly unfavorable for cation placement. This result has strong implications for the surface chemistry of 1T-MoS_2 and materials based on it, such as sensors and flexible conductors. By taking into account the uneven surface of the charged 1T-MoS2 sheet one can predict both the composition of the surface layer and the preferential placement of molecules in it.

The approach used to obtain and verify the discussed structures can reveal previously inaccessible structural features and thus can be useful for studies of similar inorganic-organic compounds with loosely coupled layers, based on metal dihalcogenides, graphene, BN etc.

Acknowledgments

This work was supported by Russian Foundation for Basic Research (RFBR) grants 12-03-00878 “A”, 14-03-00287 “A” and 13-03-12197 “ofi-m”.

References

1. T. Böker, R. Severin, A. Müller, C. Janowitz, R. Manzke, D. Voß, P. Krüger, A. Mazur, J. Pollmann, *Phys. Rev. B*, 2001, **64**, 235305.
2. K. F. Mak, C. Lee, J. Hone, J. Shan, T. F. Heinz, *Phys. Rev. Lett.*, 2010, **105**, 136805.
3. R. G. Dickinson, L. Pauling, *J. Am. Chem. Soc.*, 1923, **45**, 1466–1471.
4. D. Lembke, A. Kis, *ACS Nano*, 2012, **6**, 10070–10075.
5. H. S. S. Ramakrishna Matte, A. Gomathi, A. K. Manna, D. J. Late, R. Datta, S. K. Pati, C. N. R. Rao, *Angew. Chem.*, 2010, **122**, 4153–4156.
6. M. M. Perera, M.-W. Lin, H.-J. Chuang, B. P. Chamlagain, C. Wang, X. Tan, M. M.-C. Cheng, D. Tománek, Z. Zhou, *ACS Nano*, 2013, **7**, 4449–4458.
7. F. K. Perkins, A. L. Friedman, E. Cobas, P. M. Campbell, G. G. Jernigan, B. T. Jonker, *Nano Lett.*, 2013, **13**, 668–673.
8. C. Zhu, Z. Zeng, H. Li, F. Li, C. Fan, H. Zhang, *J. Am. Chem. Soc.*, 2013, **135**, 5998–6001.
9. D. Voiry, M. Salehi, R. Silva, T. Fujita, M. Chen, T. Asefa, V. B. Shenoy, G. Eda, M. Chhowalla, *Nano Lett.*, 2013, **13**, 6222–6227.
10. Q. Su, S. Pang, V. Alijani, C. Li, X. Feng, K. Müllen, *Adv. Mater.*, 2009, **21**, 3191–3195.
11. Y. Li, C.-Y. Xu, P. Hu, L. Zhen, *ACS Nano*, 2013, **7**, 7795–7804.
12. D. Kiriya, M. Tosun, P. Zhao, J. S. Kang, A. Javey, *J. Am. Chem. Soc.*, 2014, **136**, 7853–7856.
13. M. A. Py, R. R. Haering, *Can. J. Phys.*, 1983, **61**, 76–84.
14. R. A. Gordon, D. Yang, E. D. Crozier, D. T. Jiang, R. F. Frindt, *Phys. Rev. B*, 2002, **65**, 125407.
15. V. Petkov, S. J. L. Billinge, P. Larson, S. D. Mahanti, T. Vogt, K. K. Rangan, M. G. Kanatzidis, *Phys. Rev. B*, 2002, **65**, 092105.
16. Y. V. Zubavichus, A. S. Golub, N. D. Lenenko, Y. N. Novikov, Y. L. Slovokhotov, M. Danot, *J. Mol. Catal. Chem.*, 2000, **158**, 231–236.
17. G. Eda, T. Fujita, H. Yamaguchi, D. Voiry, M. Chen, M. Chhowalla, *ACS Nano*, 2012, **6**, 7311–7317.
18. J. Heising, M. G. Kanatzidis, *J. Am. Chem. Soc.*, 1999, **121**, 11720–11732.
19. R. Kappera, D. Voiry, S. E. Yalcin, B. Branch, G. Gupta, A. D. Mohite, M. Chhowalla, *Nat. Mater.*, 2014, **13**, 1128–1134.

20. M. Kan, J. Y. Wang, X. W. Li, S. H. Zhang, Y. W. Li, Y. Kawazoe, Q. Sun, P. Jena, *J. Phys. Chem. C*, 2014, **118**, 1515–1522.
21. Y.-C. Lin, D. O. Dumcenco, Y.-S. Huang, K. Suenaga, *Nat. Nanotechnol.*, 2014, **9**, 391–396.
22. X. Wang, X. Shen, Z. Wang, R. Yu, L. Chen, *ACS Nano*, 2014, **8**, 11394–11400.
23. V. Sánchez, E. Benavente, M. A. Santa Ana, G. González, *Chem. Mater.*, 1999, **11**, 2296–2298.
24. H. Tachibana, Y. Yamanaka, H. Sakai, M. Abe, M. Matsumoto, *Chem. Mater.*, 2000, **12**, 854–856.
25. N. D. Lenenko, E. N. Semina, V. I. Zaikovskii, A. S. Golub, *Mater. Chem. Phys.*, 2013, **141**, 35–41.
26. G. Cetnarowski, G. W. Leach, *Langmuir*, 2006, **22**, 8995–9001.
27. B. A. Vanchura, P. He, V. Antochshuk, M. Jaroniec, A. Ferryman, D. Barbash, J. E. Fulghum, S. D. Huang, *J. Am. Chem. Soc.*, 2002, **124**, 12090–12091.
28. L. F. Flores-Ortiz, M. A. Cortés-Jácome, C. Ángeles-Chávez, J. A. Toledo-Antonio, *Sol. Energy Mater. Sol. Cells*, 2006, **90**, 813–824.
29. A. S. Golub, V. I. Zaikovskii, N. D. Lenenko, M. Danot, Y. N. Novikov, *Russ. Chem. Bull.*, 2004, **53**, 1914–1923.
30. X. Rocquefelte, F. Boucher, P. Gressier, G. Ouvrard, P. Blaha, K. Schwarz, *Phys. Rev. B*, 2000, **62**, 2397–2400.
31. H. S. S. R. Matte, U. Maitra, P. Kumar, B. Govinda Rao, K. Pramoda, C. N. R. Rao, *Z. Für Anorg. Allg. Chem.*, 2012, **638**, 2617–2624.
32. L. Wang, Z. Xu, W. Wang, X. Bai, *J. Am. Chem. Soc.*, 2014, **136**, 6693–6697.
33. B. E. Warren, *Phys. Rev.*, 1941, **59**, 693–698.
34. K. Ufer, G. Roth, R. Kleeberg, H. Stanjek, R. Dohrmann, J. Bergmann, *Z. Für Krist. J. Struct. Phys. Chem. Asp. Cryst. Mater.*, 2004, **219**, 519–527.
35. X. Wang, J. Li, R. D. Hart, A. van Riessen, R. McDonald, *J. Appl. Crystallogr.*, 2011, **44**, 902–910.
36. X. Wang, R. D. Hart, J. Li, R. G. McDonald, A. van Riessen, *J. Appl. Crystallogr.*, 2012, **45**, 1295–1302.
37. L. Houben, A. N. Enyashin, Y. Feldman, R. Rosentsveig, D. G. Stroppa, M. Bar-Sadan, *J. Phys. Chem. C*, 2012, **116**, 24350–24357.
38. F. Wypych, R. Schöllhorn, *J. Chem. Soc. Chem. Commun.*, 1992, 1386.
39. F. Allen, *Acta Crystallogr. Sect. B*, 2002, **58**, 380–388.
40. R. F. W. Bader, *Atoms in Molecules: A Quantum Theory*, Oxford University Press, USA, 1994.
41. E. Espinosa, E. Molins, C. Lecomte, *Chem. Phys. Lett.*, 1998, **285**, 170–173.
42. E. Espinosa, C. Lecomte, E. Molins, *Chem. Phys. Lett.*, 1999, **300**, 745–748.
43. E. Espinosa, E. Molins, *J. Chem. Phys.*, 2000, **113**, 5686.
44. K. A. Lyssenko, *Mendeleev Commun.*, 2012, **22**, 1–7.
45. N. G. Naumov, A. A. Korlyukov, D. A. Piryazev, A. V. Virovets, V. E. Fedorov, *Russ. Chem. Bull.*, 2013, **62**, 1852–1857.
46. A. S. Goloveshkin, I. S. Bushmarinov, N. D. Lenenko, M. I. Buzin, A. S. Golub, M. Y. Antipin, *J. Phys. Chem. C*, 2013, **117**, 8509–8515.
47. A. S. Golub, Y. V. Zubavichus, Y. L. Slovokhotov, Y. N. Novikov, M. Danot, *Solid State Ion.*, 2000, **128**, 151–160.
48. Bruker, *TOPAS 4.2 User Manual*, Bruker AXS GmbH, Karlsruhe, Germany, 2009.